

Journal of Seismic Exploration

ARTICLE

Efficient wave-equation-based Kirchhoff-style migration using interpolated excitation information

Sumin Kim¹, Jiho Ha², and Wookeen Chung¹*

¹Department of Energy and Resources Engineering, National Korea Maritime and Ocean University, Busan, South Korea

²Pohang Branch, Korea Institute of Geoscience and Mineral Resources (KIGAM), Pohang, South Korea

Abstract

Reverse time migration is widely recognized as one of the most advanced seismic depth migration techniques because of its ability to generate a high-quality seismic image even for complex structures. However, its practical implementation for large-scale applications can be hindered by tremendous computational overhead and memory demands associated with handling wavefields. To address these challenges, we propose a wave equation-based, Kirchhoff-style migration method incorporating the excitation amplitude imaging condition. In our migration scheme, both the forward and backward wavefields are represented using excitation information obtained by interpolating a limited set of excitation information. This representation allows us to avoid not only storing the forward wavefield but also performing backward wavefield simulation. Numerical experiments with both synthetic and field data demonstrate that the proposed migration approach can deliver high-quality migration images with significantly improved computational efficiency.

Keywords: Seismic migration; Computational efficiency; Seismic imaging

*Corresponding author: Wookeen Chung (wkchung@kmou.ac.kr)

Citation: Kim S, Ha J, Chung W. Efficient wave-equation-based Kirchhoff-style migration using interpolated excitation information. *J Seismic Explor*. 2025;34(3):49-60. doi: 10.36922/JSE025320055

Received: August 9, 2025
Revised: September 4, 2025
Accepted: September 11, 2025

Published online: October 8, 2025

Copyright: © 2025 Author(s). This is an Open-Access article distributed under the terms of the Creative Commons Attribution License, permitting distribution, and reproduction in any medium, provided the original work is properly cited.

Publisher's Note: AccScience Publishing remains neutral with regard to jurisdictional claims in published maps and institutional affiliations

1. Introduction

Seismic depth migration has become an essential technique for revealing complex geological structures in the subsurface. With breakthroughs in computing technology, various seismic depth migration techniques have been intensively developed in recent decades, including Kirchhoff migration approaches, Gaussian beam migration approaches, and one-way wave equation migration approaches. Among these seismic depth migration techniques, reverse-time migration (RTM), based on a two-way wavefield simulation engine, is regarded as the most accurate technique in seismic imaging, since it can handle steeply dipping structures as well as various wave types such as reflections and diffractions. Thus, RTM can provide high-quality seismic images in complicated media.

Despite the excellent performance of RTM, its practical implementation has inherent limitations due to its high computational cost. The primary contributor to this cost is the large amount of memory required for saving the forward wavefield.

Generally, the basic procedure of RTM consists of the following procedures: the forward wavefield simulation with source function, backward wavefield simulation with the recorded seismograms, and construction of the migration image based on the imaging condition. During the application of the imaging condition, huge memory resources may be required. To generate the seismic image from RTM, the temporal history of the forward wavefield at every imaging time step should be accessible. Since the dimension of the entire forward wavefield is determined by the model dimensions and imaging time steps in wavefield simulation, huge memory resources are needed to save the forward wavefield. Of course, for small-scale applications, memory devices or disk input/output (I/O) may be sufficient to store the forward wavefield. However, for large-scale applications, alternative strategies for handling forward wavefield during the imaging condition procedure are required to alleviate the computational costs.

To address this computational burden associated with storing the forward wavefield in RTM, many wavefield reconstruction-based approaches have been investigated. One widely adopted method is forward wavefield reconstruction. ¹²⁻¹⁴ In this approach, the forward wavefield is stored only on the model boundaries during forward simulation and then reconstructed during backward simulation. This strategy is memory-efficient because only a few grid points are required to store the forward wavefield; however, it necessitates additional wavefield simulations.

To further reduce the memory requirements for storing the forward wavefield, Nguyen and McMechan¹⁵ proposed the excitation amplitude (ExA) imaging condition. In the ExA imaging condition for RTM, the maximum amplitude of the forward wavefield and its associated travel time are referred to as the ExA and the excitation time (ExT), respectively. RTM with the ExA imaging condition can generate the migration image efficiently, as the ExA and ExT are represented by a single value for each grid point in the model. Owing to this memory-efficient advantage, ExA imaging condition has been applied not only in acoustic RTM¹⁵⁻¹⁷ but also in elastic RTM.^{18,19} Furthermore, Kalita and Alkhalifah²⁰ modified the ExA imaging condition by incorporating source information, in which the source wavelet is used to represent the forward wavefield. This modified ExA imaging condition has been employed in a wide range of inversion-based seismic imaging techniques, including full waveform inversion,21,22 and least-squares RTM.^{23,24}

Following Kalita and Alkhalifah,²⁰ we develop a waveequation-based Kirchhoff-style migration based on excitation representation, in which the backward as well as the forward wavefield are represented using excitation information. Thus, no backward wavefield simulation is needed in our migration scheme if excitation information at the receiver position is available. To enhance computational efficiency, we perform a limited number of forward wavefield simulations and use interpolation to generate the excitation information, rather than performing forward wavefield simulations for each receiver position. This interpolated excitation information enables migration to be implemented without backward wavefield simulation.

In this paper, we first introduce the conventional RTM, followed by wavefield representation using excitation information. We then develop a wave-equation-based, Kirchhoff-style migration method using excitation representation and derive a modified imaging condition for practical implementation. Finally, we present both a synthetic example and a field application to demonstrate the efficiency and practicability of the proposed migration approach.

2. Methodology

2.1. Review of RTM

Prestack RTM comprises three procedures: (i) forward wavefield simulation using the source function, (ii) backward wavefield simulation using the recorded seismograms, and (iii) application of an imaging condition. Assuming a 2D isotropic acoustic environment, both the forward and backward wavefield simulations for prestack RTM can be computed from the following two equations:

$$\left(\frac{1}{c^2}\frac{\partial^2}{\partial t^2} - \nabla^2\right) S(t, \mathbf{x}; \mathbf{x}_s) = f(t; \mathbf{x}_s), \#$$
 (I)

And

$$\left(\frac{1}{c^2}\frac{\partial^2}{\partial t^2} - \nabla^2\right) R(t, \mathbf{x}; \mathbf{x}_s) = d(T - t, \mathbf{x}_r; \mathbf{x}_s), \#$$
(II)

Where c is migration velocity, ∇^2 denotes Laplacian operator, x is imaging point, \mathbf{x}_s is shot position, t is time, T is maximum time, S(t, x; \mathbf{x}_s) and R(t, x; \mathbf{x}_s) are forward and backward wavefields, respectively. f(t; \mathbf{x}_s) is the source function injecting at the source position \mathbf{x}_s , and d(t, \mathbf{x}_r ; \mathbf{x}_s) is recorded seismogram at receiver position \mathbf{x}_r . Following the forward wavefield simulation, the migration image is computed by applying the imaging condition with the forward and backward wavefields. In this study, a zero-lag cross-correlation imaging condition is used and defined as follows:

$$I(\mathbf{x};\mathbf{x}_s) = \int_0^T S(t,\mathbf{x};\mathbf{x}_s) R(T-t,\mathbf{x};\mathbf{x}_s) dt,$$
(III)

Where I(x; x_s) represents migration image at x. **Equation III** implies that both the forward and backward wavefields must be available simultaneously at each imaging time step. A straightforward way to make the forward wavefield available during the application of the imaging condition is to store it in memory or write it to disk and read it back during the backward wavefield simulation. However, this approach incurs tremendous memory and I/O time costs. This limitation poses a major obstacle to the practical implementation of RTM for large-scale applications, particularly in 3D seismic imaging.

2.2. Representation of forward and backward wavefield using excitation information

According to the theory of ExA imaging condition in RTM,¹⁵ the most energetic amplitude and its arrival time at each grid point in model space are defined as ExA and excitation time (ExT), respectively. This relationship can be expressed as follows:

$$t_e(\mathbf{x}; \mathbf{x}_s) = \underset{\cdot}{\operatorname{argmin}}(|S(t, \mathbf{x}; \mathbf{x}_s)|), \#$$
 (IV)

And

$$S_{e}(t, \mathbf{x}; \mathbf{x}_{s}) = S(t, \mathbf{x}; \mathbf{x}_{s})\delta(t - t_{e}(\mathbf{x}; \mathbf{x}_{s})), = \begin{cases} S(t, \mathbf{x}; \mathbf{x}_{s}), & \text{for } t = t_{e} \\ 0, & \text{otherwise} \end{cases}$$
(V)

Where t_e is the ExT at grid point x, δ is Dirac delta function, and $S_e(t, x; x_s)$ is the ExA of the forward wavefield $S(t, x; x_s)$. The ExA can efficiently generate a migration image because it stores only one snapshot to represent the forward wavefield. With ExA and ExT, the reconstructed forward wavefield $\hat{S}_e(t, x; x_s)$ can be represented by convolving the source wavelet as follows:

$$\hat{S}_{e}(t, \mathbf{x}; \mathbf{x}_{s}) = G(t, \mathbf{x}; \mathbf{x}_{s}) \delta(t - t_{e}(\mathbf{x}; \mathbf{x}_{s})) * f(t), #$$
(VI)

Where $G(t, x; x_s)$ is Green's function propagating in the migration velocity c, and * represents the temporal convolution operator. For simplicity, **Equation VI** can be expressed in compact matrix form as follows:

$$\hat{S}_{e} = Wu_{\delta}, \#$$
 (VII)

Where $\hat{\mathbf{S}}_e \in \mathbb{R}^{N \times 1}$ stands for represented forward wavefield using excitation information, and N is the number of time samples. Causal convolution matrix $\mathbf{W} \in \mathbf{R}^{\mathbf{N} \times \mathbf{N}}$ is constructed by source wavelet f(t) with lower triangular Toeplitz structure as follows:

$$W = \begin{bmatrix} f_1 & 0 & \cdots & 0 & 0 \\ f_2 & f_1 & \cdots & 0 & 0 \\ \vdots & \vdots & \ddots & \vdots & 0 \\ f_{N-1} & f_{N-2} & \cdots & f_1 & 0 \\ f_N & f_{N-1} & \cdots & f_2 & f_1 \end{bmatrix}, \#$$
(VIII)

And $u_-\delta \in \mathbb{R}^{N\times 1}$ is a vector with a single non-zero element $G(t_e(x;x_s))$ at N_{t_e} indicating integer time step of $t_e(x;x_s)$.

In the same manner, the backward wavefield can also be reconstructed using a recorded seismogram with excitation information if excitation information is available at the receiver position \mathbf{x}_r is available. The reconstructed backward wavefield can be expressed as follows:

$$\hat{R}_{e}(t,\mathbf{x};\mathbf{x}_{s}) = G(t,\mathbf{x};\mathbf{x}_{r})\delta(t - t_{e}(\mathbf{x};\mathbf{x}_{r})) * d(T - t;\mathbf{x}_{r}), #$$
(IX)

Where $\hat{R}_e(t, \mathbf{x}; \mathbf{x}_s)$ is the reconstructed backward wave field. This Equation IX can be also written as compact matrix form for simplicity as follows:

$$\hat{R}_{e} = V_{\delta}Rd,\# \tag{X}$$

Where $\hat{R}_e \in \mathbb{R}^{N \times N}$ stands for represented backward wavefield using excitation information. $V^\delta \in R^{N \times N}$ is causal convolution matrix with $G(t, x; x_r)\delta(t-t_e(x; x_r))$. Time reverse matrix $R \in R^{N \times N}$ and trace vector of the recorded seismogram $d \in R^{N \times 1}$ can be expressed as follows:

$$R = \begin{bmatrix} 0 & 0 & \cdots & 0 & 1 \\ 0 & 0 & \cdots & 1 & 0 \\ \vdots & \vdots & \ddots & \vdots & 0 \\ 0 & 1 & \cdots & 0 & 0 \\ 1 & 0 & \cdots & 0 & 0 \end{bmatrix}, \#$$
(XI)

And

$$d = [d_1, d_2, \dots, d_{N-1}, d_N]^T, \#$$
(XII)

Where superscript T represents the transpose operation.

2.3. Wave-equation-based Kirchhoff-style migration using interpolated excitation information (WEKM-IEI)

We propose a new imaging condition based on the backward as well as the forward wavefield representations using excitation information. By substituting **Equations VI** and **IX** into **Equation III**, the new imaging condition can be expressed as follows:

$$I_{e}(\mathbf{x}; \mathbf{x}_{s}) = \int_{0}^{T} \hat{S}_{e}(t, \mathbf{x}; \mathbf{x}_{s}) \hat{R}_{e}(T - t, \mathbf{x}; \mathbf{x}_{s}) dt.$$
 (XIII)

Based on this imaging condition, the migration image can be computed by using excitation representations of the forward and backward wavefields. In other words, backward wavefield simulation is unnecessary for the migration procedure if excitation information at receiver position \mathbf{x}_r is available. However, in the practical implementation of WEKM-IEI, **Equation XIII** should be modified to take advantage of the ExA imaging condition. To modify **Equation XIII**, in the same manner as Kalita and Alkhalifah,²⁰ we can express our imaging condition in matrix form using **Equations VII** and **X** as follows:

$$I_e(x) = \langle Wu_\delta, RV_\delta Rd \rangle, \#$$
 (XIV)

Where \langle , \rangle represents the dot product operation. With the aid of properties of the dot product and some algebra, we can derive the final equation for our imaging condition as:

$$I_{c}(\mathbf{x}) = \mathbf{u}_{c}, \mathbf{V}^{T} \mathbf{W}^{T} \mathbf{d}.$$
 (XV)

The detailed derivation of above **Equation XV** is presented in the Appendix. For simplicity, **Equation XV** can be expressed as follows:

$$I_e(\mathbf{x}) = \mathbf{u}_{\delta}, \mathbf{V}_{\delta}^{\mathrm{T}} \hat{\mathbf{d}}, \#$$
 (XVI)

Where $\hat{\mathbf{d}} = \mathbf{W}^T \mathbf{d}$ represents the recorded seismogram cross-correlated with the source wavelet f(t). This equation suggests that explicit cross-correlation between the excitation representation of the Green's function at receiver position \mathbf{x}_r and $\hat{\mathbf{d}}$ may be required for constructing the migration image. However, since the temporal cross-correlation matrix \mathbf{V}_δ^T consists of the time-shifted Dirac delta function with scaled amplitude $G(\mathbf{t}_e(\mathbf{x}; \mathbf{x}_s))$, it also acts as the time shifter. Furthermore, \mathbf{u}^δ has only a single non-zero element scaled by $G(\mathbf{t}_e(\mathbf{x}; \mathbf{x}_s))$. Thus, the dot product operation of **Equation XVI** takes only a few floating-point operations per second. Therefore, the calculation of the migration image for our approach is expressed as:

$$I_{e}(\mathbf{x}) = G(t_{e}(\mathbf{x}; \mathbf{x}_{s}))G(t_{e}(\mathbf{x}; \mathbf{x}_{r}))\hat{d}(t_{e}(\mathbf{x}; \mathbf{x}_{s}) + t_{e}(\mathbf{x}; \mathbf{x}_{r})).\#$$
(XVII)

To further improve the computational efficiency of our approach, we interpolate the excitation information from just a part of the excitation information. For representation of the backward wavefield at each receiver position \mathbf{x}_r , the excitation information at each receiver position \mathbf{x}_r should be available. Intuitively, it can be generated from

the wavefield simulation. However, massive computations are inevitable because hundreds of receivers are usually exploited by shots in the seismic survey. Hence, rather than generating excitation information at each receiver position, we construct the excitation information by applying an interpolation method to a part of it. From this interpolated excitation information, the forward and backward wavefields can be represented. Consequently, the WEKM-IEI can construct a migration image efficiently. The algorithm in the Appendix shows the implementation of our migration approach in detail. Based on the ExA imaging condition, the WEKM-IEI also has a memory advantage for saving the forward wavefield. In addition, as mentioned before, there is no need to perform the backward wavefield simulation in the WEKM-IEI. Consequently, the WEKM-IEI can provide a high-quality migration image with less computational cost as well as memory requirements.

3. Numerical examples

In this section, we first verify the reconstruction of the forward and backward wavefield using excitation information, followed by the feasibility of our migration approach by comparing the conventional RTM on a modified Marmousi2 velocity model. After that, we apply the WEKM-IEI to a field seismic dataset. In these numerical examples, we exploit the finite difference scheme with O(2, 12) accuracy in the temporal and spatial domains with CPML boundary condition²⁵ at four edges to attenuate nonphysical reflections from the model boundaries, including the free surface. All numerical examples are performed using 25 CPUs (Intel Xeon Gold 5218R CPU with 2.10 GHz).

3.1. Synthetic test

To verify the accuracy of the forward and backward wavefields reconstructed by excitation information, we use the modified Marmousi2 velocity model shown in Figure 1A. This velocity model is discretized by 401×176 grids, with 10-m horizontal and vertical grid intervals, respectively. To generate the migration velocity model, a 2D Gaussian filter with a $600 \text{ m} \times 600 \text{ m}$ window is applied to the true velocity model. The migration velocity model is shown in Figure 1B. In these wavefield reconstruction tests, the single shot is located at 2 km in the horizontal direction. 15 Hz Ricker wavelet is used as the source wavelet.

As the first wavefield reconstruction test, Figure 2A and B shows snapshots of the true and reconstructed forward wavefields from excitation information, respectively. We can find that the reconstructed forward wavefield is almost identical to the true one, except for the reflected wavefield.

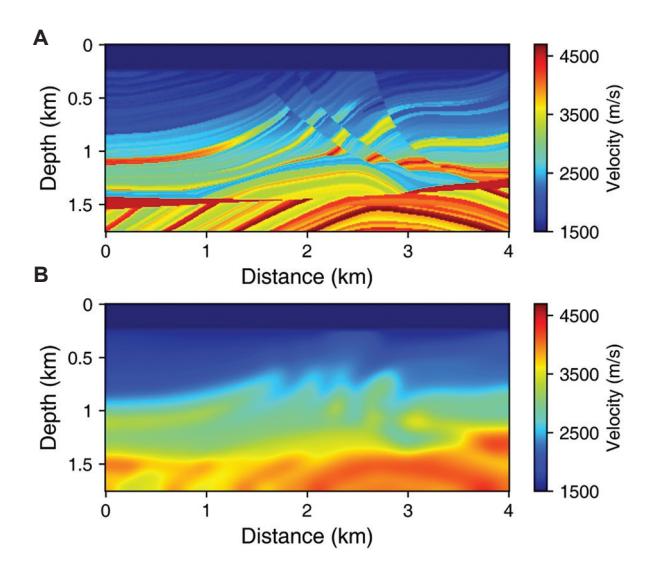


Figure 1. True modified Marmousi2 velocity model (A) and migration velocity model (B)

To compare these snapshots in detail, traces of the true and reconstructed forward wavefields are extracted at 2, 0.5 km in distance and depth directions, respectively (Figure 3). Note that the main wave in the forward wavefield is accurately reconstructed from excitation information. Although the forward wavefield reconstructed by excitation information contains only the transmitted wave due to the inherent limitation of the ExA method, wavefield representation using excitation information can provide a reliable forward wavefield.

For another wavefield reconstruction test for the backward wavefield, a seismogram is obtained from a receiver located at the same position of the shot. Direct wave is removed in the recorded seismogram for the backward wavefield reconstruction test. Figure 4A and B illustrate the snapshots of the true and reconstructed backward wavefields from excitation information, respectively. The reconstructed backward wavefield is also identical to the true one. For a more detailed comparison between the true and reconstructed backward wavefields, the traces from those wavefields are extracted at 2, 0.6 km in distance and depth directions, respectively (Figure 5). The trace of the reconstructed backward wavefield represents the true backward wavefield accurately. From these wavefield reconstruction tests, excitation information can be exploited to represent the backward and the forward wave fields with high accuracy.

We now verify the feasibility of the WEKM-IEI. For the implementation of the WEKM-IEI, the ExA and corresponding ExT maps should be constructed for each source and receiver position. Although this excitation

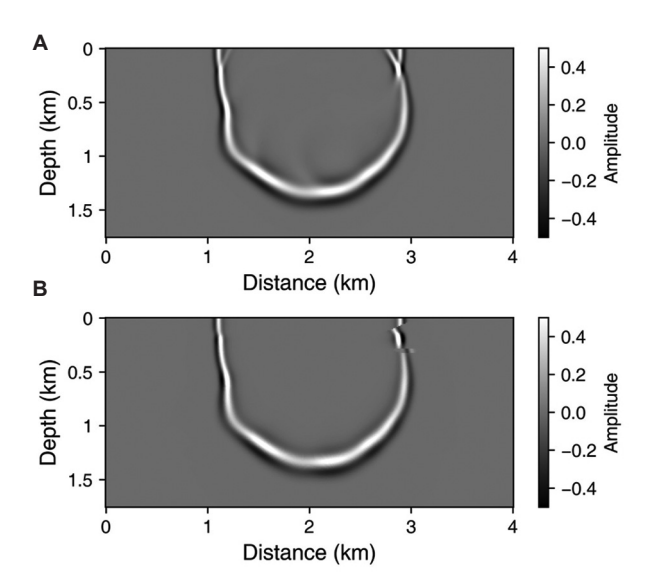


Figure 2. Forward wavefields in the migration velocity model (Figure 1B) obtained by full wavefield modeling (A) and excitation representation (B)

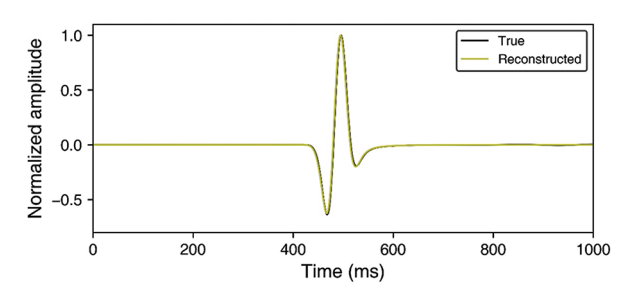


Figure 3. Traces of forward wavefields in the migration velocity model (Figure 2A and B) extracted at (x,z) = (2, 0.5) km

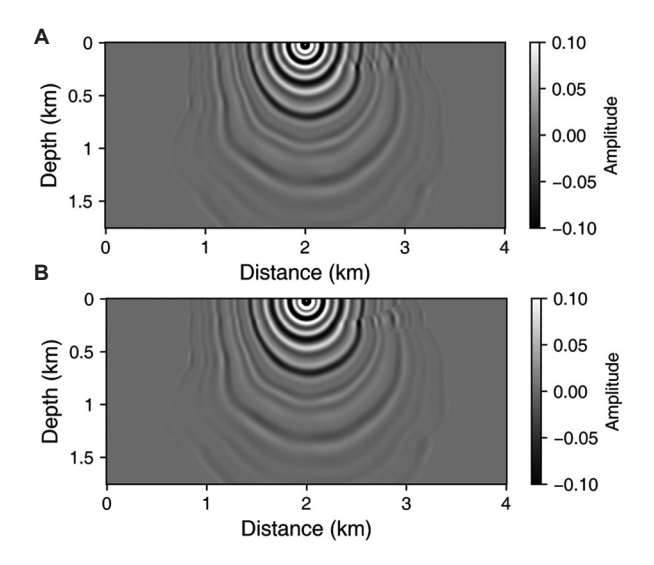


Figure 4. Backward wavefields in the migration velocity model (Figure 1B) obtained by full wavefield modeling (A) and excitation representation (B)

information can be generated by implementing forward wavefield simulations at each source and receiver position, it leads to tremendous computing costs. As mentioned above, we construct excitation information using the interpolation method to alleviate the computing cost. First, we generate some of the excitation information by implementing forward wavefield simulations. In this synthetic example, 81 shots are deployed evenly from 0 to 4 km with a 0.05 km shot interval. In other words, only 20% of excitation information is generated using the forward wavefield simulation. For constructing the entire

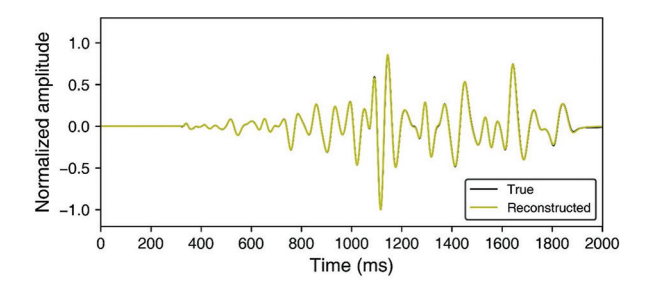


Figure 5. Traces of backward wavefields in the migration velocity model (Figure 4A and B) extracted at (x,z) = (2,0.6) km

excitation information, an L2-norm-based interpolation method with small fraction of excitation information is performed to fill the missing excitation information. The L2-norm-based interpolation used in this paper can be expressed as follows:

$$\min_{m} m - Sm_{2}^{'2} + \lambda Rm_{2}^{'2}, \#$$
 (XVIII)

m is the decimated excitation information generated from the forward wavefield simulation, m' is excitation information needed to be reconstructed, S is sampling matrix, λ is the penalty coefficient (determined empirically), and R is the regularization matrix (the second-derivative operator used in this paper). Although the excitation information for our migration approach is three-dimensional, Equation XVIII is expressed in matrix form, i.e., for a two-dimensional dataset. To reconstruct the excitation information, we solve Equation XVIII independently for each depth slice of the decimated excitation volume.

Figures 6 and 7 show the three different ExA and the corresponding ExT to verify the accuracy of interpolated excitation information: (a) true excitation information, (b) some of the excitation information generated by

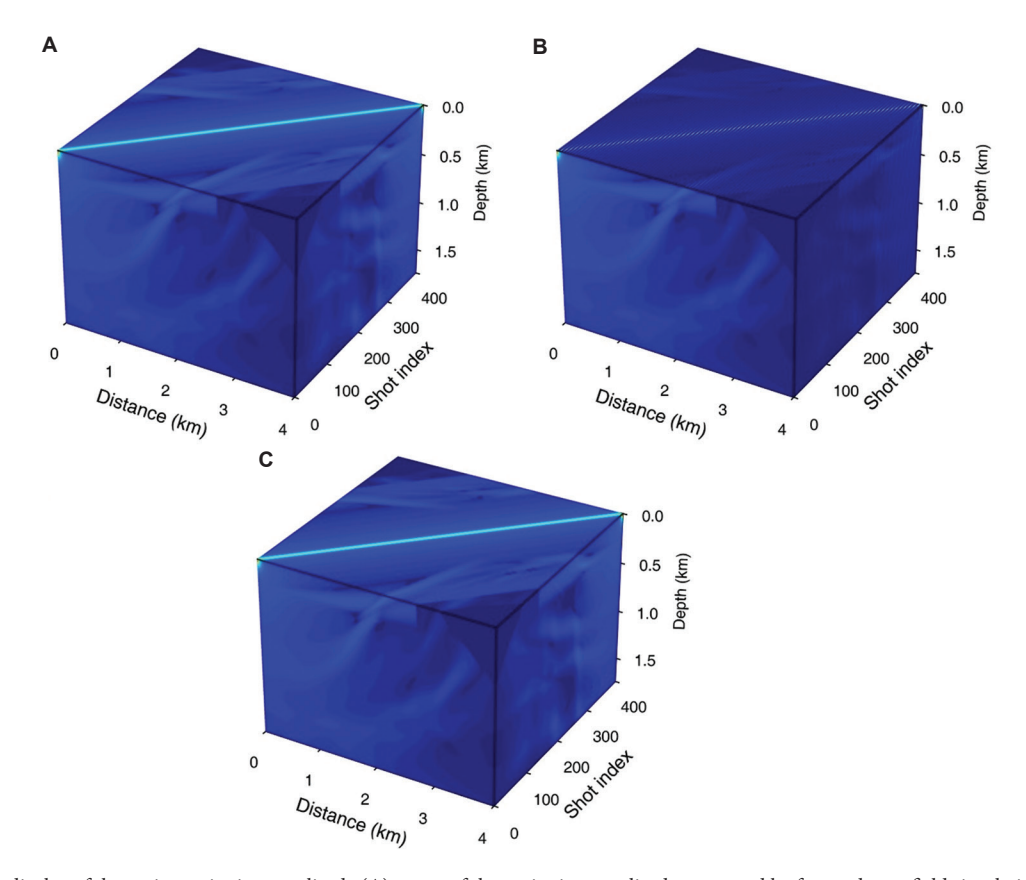


Figure 6. 3D display of the entire excitation amplitude (A), some of the excitation amplitude generated by forward wavefield simulation (B), and the interpolated excitation amplitude (C)

Volume 34 Issue 3 (2025) 54 doi: 10.36922/JSE025320055

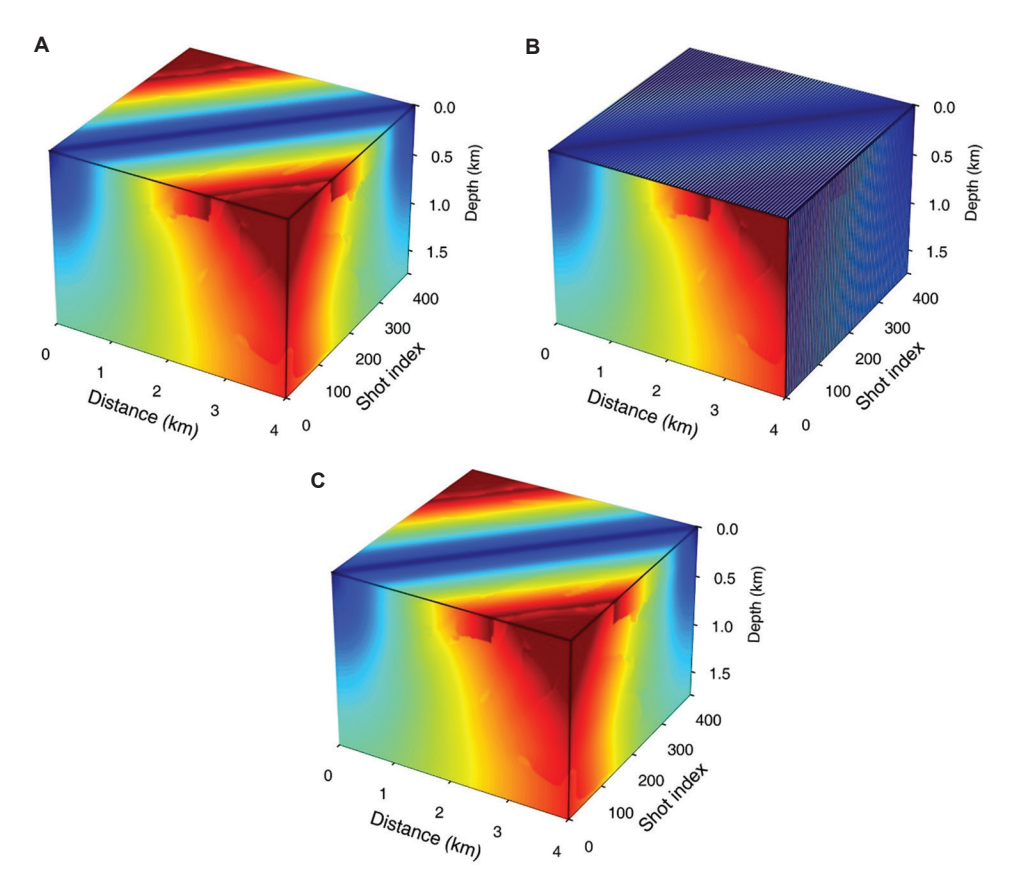


Figure 7. 3D display of (A) the entire excitation time, (B) some of the excitation time generated by forward wavefield simulation, (C) the interpolated excitation time

forward wavefield simulation, and (c) interpolated excitation information, respectively. It is noted that the interpolated excitation information is almost identical to true excitation information, despite using only 20% of the entire excitation information.

Next, we compare the migration images obtained from conventional RTM and the WEKM-IEI. To generate the recorded seismogram, 201 sources are distributed from 0 to 4 km with a horizontal interval of 0.02 km. A total of 401 receivers, evenly spaced from 0 to 4 km with a horizontal interval of 0.01 km, record the seismogram for 2 s at a temporal sampling interval of 1 ms. To avoid the massive memory usage for saving the forward wavefield in conventional RTM, a source wavefield reconstruction method is adopted.¹³ A high-pass filter is applied to the migration image as a post-processing procedure. Figure 8A and B present the migration images of conventional RTM and the WEKM-IEI, respectively. It is noted that the WEKM-IEI provides a high-quality migration image similar to that of conventional RTM for a complex structural velocity model, even when using interpolated ExA and the corresponding ExT. For further comparison, depth profiles are extracted at 1 and

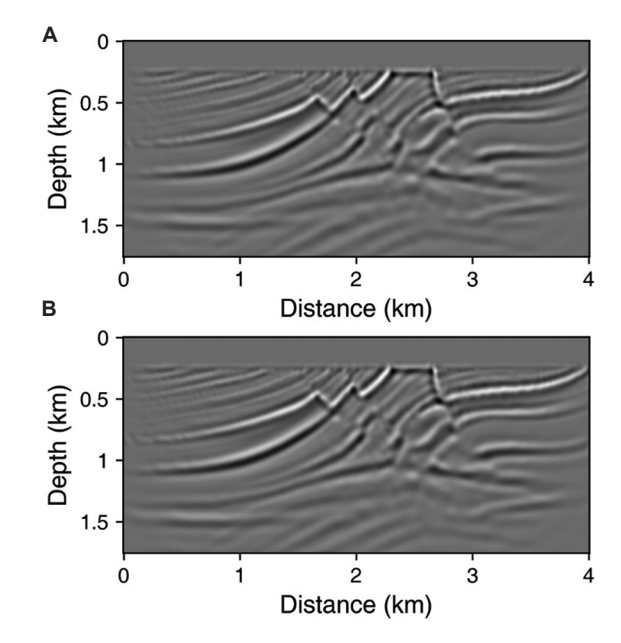


Figure 8. Migration images obtained from conventional RTM (A) and WEKM-IEI (B)

Abbreviations: RTM: Reverse time migration; WEKM-IEI: Wave-equation based Kirchhoff-style migration using interpolated excitation information.

2 km in the distance direction (Figure 9). The reflectors of conventional RTM and the WEKM-IEI are almost identical.

Table 1 displays the memory requirements and computing times of conventional RTM and the WEKM-IEI. In the WEKM-IEI, only 0.16 GB, approximately 12.14% over conventional RTM using the source reconstruction method, is required. It is obvious that the WEKM-IEI requires less memory storage than conventional RTM using the source wavefield reconstruction method, since it requires no saving of the entire time history of the wavefield during migration. The source wavefield reconstruction method in RTM can also reduce the memory requirement, but additional wavefield simulation during backward wavefield simulation should be implemented. Thus, it spends extra computing time. In contrast, the WEKM-IEI can omit the backward wavefield simulation using interpolated excitation information to represent both forward and backward wavefields. This strength leads to high computational efficiency.

4. Field application

We present a field application to investigate the practicability of the WEKM-IEI. In this field application, 2D shallow marine seismic data with 16 channels, acquired by Korea Institute of Geoscience and Mineral Resources (KIGAM), were used. The imaging profile has a distance of 1,000 m and a depth of 60 m. The velocity model ranging from 1,500 to 1,800 m/s was discretized by 1601×97 grids in distance and depth direction with the grid intervals of both 0.625 m. 300 shots were evenly distributed with an interval of approximately 3.125 m, and each of them had 16 receivers with a streamer configuration. The recording time length of this field data is 1.5 s. Instead of estimating the source wavelet, we convolved the known wavelet with the field data,26 which has a Tukey-shaped at 20-100-400-500 Hz. For the implementation of our migration approach, 161 shots, distributed evenly from 0 to 1 km with a shot interval of 6.25 m, were exploded to generate some of the excitation information. Afterward, L2-norm-based interpolation was implemented to fill the missing excitation information.

Figure 10A and B represent the migration images using conventional RTM and the WEKM-IEI, respectively. From these migration results, we can notice that the migration image obtained from the WEKM-IEI exhibits an almost identical migration image using conventional RTM. To compare these migration images in detail, two profiles in depth direction are extracted at 0.3 and 0.8 km in distance direction (Figure 11A and B). The reflectors in both RTM and the WEKM-IEI are nearly identical.

Table 2 shows the computational costs for required memory and computing times of conventional RTM and the

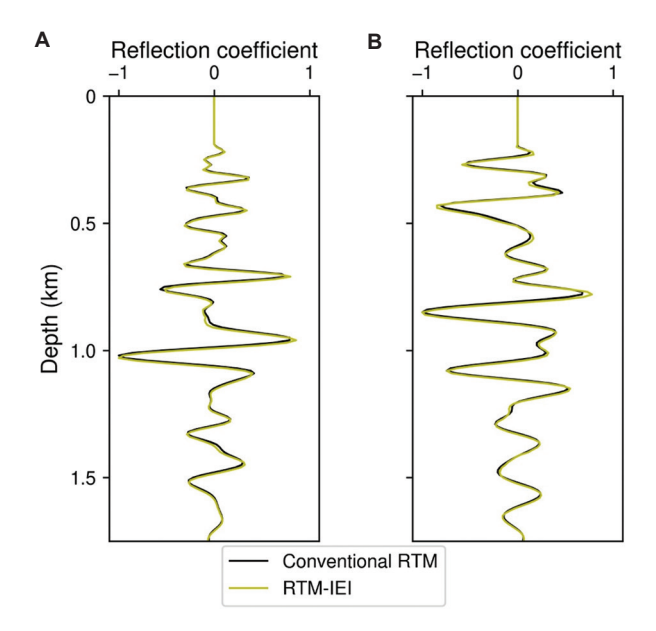


Figure 9. Comparisons between depth profiles of conventional RTM and WEKM-IEI extracted at 1 and 2 km in the distance direction Abbreviations: RTM: Reverse time migration; WEKM-IEI: Wave-equation based Kirchhoff-style migration using interpolated excitation information.

Table 1. Computational costs of conventional RTM and WEKM-IEI

Method	Required memory (GB)	Computing time (s)
Conventional RTM	1.30	386.15
WEKM-IEI	0.16	80.65

Notes: Computing required memory: 1) conventional RTM = $(2 \cdot ((nx \cdot n) + (nz \cdot n)) \cdot (nt \cdot 2) + 2 \cdot (nx \cdot nz)) \cdot ncpu \cdot 4$ bytes, 2) WEKM-IEI = $(nx \cdot nz \cdot nx) \cdot (2+4)$ bytes (nx, nz): The number of x- and z-direction grids; n: Additional grid determined by special accuracy order in wavefield simulation; nt: Time steps; ncpu: Number of cpus. Abbreviations: RTM: Reverse time migration;

WEKM-IEI: Wave-equation based Kirchhoff-style migration using interpolated excitation information.

Table 2. Computational costs of conventional RTM and WEKM-IEI

Method	Required memory (GB)	Computing time (s)
Conventional RTM	0.59	128.07
WEKM-IEI	0.043	181.02

Notes: Computing required memory: 1) conventional

 $RTM = (2 \cdot ((nx_sub\cdot n) + (nz\cdot n)) \cdot (nt \cdot 2) + 2 \cdot (nx_sub\cdot nz)) \cdot ncpu\cdot 4 \ bytes, 2) \\ WEKM-IEI = (nx_sub\cdot nz\cdot n_coposition) \cdot (2+4) \ bytes, (nx_sub: The number of x-grid (practical area for wavefield simulation), n_coposition: Number of co-location of source and receivers in model space.$

Abbreviations: RTM: Reverse time migration;

WEKM-IEI: Wave-equation-based Kirchhoff-style migration using interpolated excitation information.

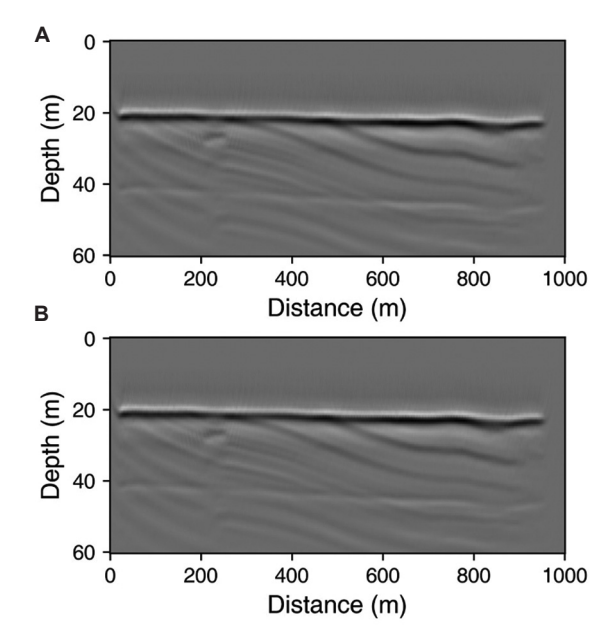


Figure 10. Migration results of field application: (A) conventional RTM and (B) WEKM-IEI

Abbreviations: RTM: Reverse time migration; WEKM-IEI: Wave-equation based Kirchhoff-style migration using interpolated excitation information.

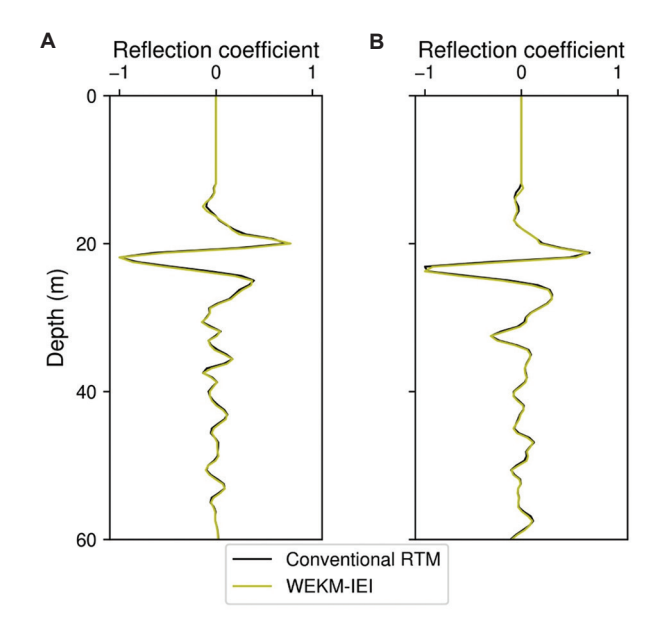


Figure 11. Depth profiles of conventional RTM and WEKM-IEI extracted at 0.3 km (A) and 0.8 km (B) in the distance direction Abbreviations: RTM: Reverse time migration; WEKM-IEI: Wave-equation based Kirchhoff-style migration using interpolated excitation information.

WEKM-IEI in field application. For the required memory, WEKM-IEI requires only 0.043 GB, approximately 7.19% over conventional RTM using the source reconstruction

method. In contrast, the computational time of WEKM-IEI is higher than that of conventional RTM with source-wavefield reconstruction. In our field application, we applied an aperture in the model space for each shot based on the source and receiver positions. Because the field dataset used in this study had few receivers, the aperture-limited model domain was very small, and conventional RTM could therefore be run quickly. However, if a field dataset with many receivers is used, conventional RTM with source-wavefield reconstruction would incur substantial computational cost.

5. Conclusion

Through this work, we propose wave-equationbased Kirchhoff-style migration approach for further improvements of computational efficiency based on the excitation imaging condition. This new migration approach can represent both forward and backward wavefields using excitation information. However, the excitation information at receiver, as well as shot positions, is required. In this work, we implemented a small number of forward wavefield simulations and interpolation to generate excitation information. Using interpolated excitation information yields high-quality migration images while improving efficiency by reducing memory requirements for storing the forward wavefield and cutting computational costs through the omission of backward wavefield simulation. Synthetic data test demonstrates that our migration approach can provide a similar migration image compared to that of conventional RTM, but its computational efficiency is higher than that of conventional RTM. Subsequent field application indicates the practicability of our migration approach.

Acknowledgments

None.

Funding

This research was supported by the Korea Institute of Marine Science and Technology Promotion (KIMST) funded by the Ministry of Oceans and Fisheries, Korea (RS-2023-00259633) and the Basic Research Project "Development of operation management infrastructure for TAMHAE 3 and seamless seismic technology connecting coastal areas (25–3322)" of the Korea Institute of Geoscience and Mineral Resources (KIGAM) funded by the Ministry of Science and ICT of Korea.

Conflict of interest

The authors declare they have no competing interests.

Author contributions

Conceptualization: Sumin Kim, Wookeen Chung

Data curation: Sumin Kim, Jiha Ha Formal analysis: Sumin Kim

Investigation: Sumin Kim, Wookeen Chung Methodology: Sumin Kim, Wookeen Chung

Writing-original draft: Sumin Kim, Wookeen Chung

Writing-review & editing: All authors

Availability of data

Data are available from the corresponding author on reasonable request.

References

 Zhu J, Lines LR. Comparison of Kirchhoff and reverse-time migration methods with applications to prestack depth imaging of complex structures. *Geophysics*. 1998;63(4): 1166-1176.

doi: 10.1190/1.1444416

 Gray SH, Etgen J, Dellinger J, Whitmore D. Seismic migration problems and solutions. *Geophysics*. 2001;66(5):1622-1640.

doi: 10.1190/1.1487107

3. Gray SH, May WP. Kirchhoff migration using eikonal equation traveltimes. *Geophysics*. 1994;59:810-817.

doi: 10.1190/1.1443639

4. Gray SH, Bleistein N. True-amplitude Gaussian-beam migration. *Geophysics*. 2009;74(2):S11-S23.

doi: 10.1190/1.3052116

5. Hill NR. Prestack Gaussian-beam depth migration. *Geophysics*. 2001;66(4):1240-1250.

doi: 10.1190/1.1487071

6. Mulder WA, Plessix RE. A comparison between one-way and two-way wave-equation migration. *Geophysics*. 2004;69(6):1491-1504.

doi: 10.1190/1.1836822

7. Zhang Y, Zhang G, Bleistein N. Theory of true-amplitude one-way wave equations and true-amplitude common-shot migration. *Geophysics*. 2005;70(4):E1-E10.

doi: 10.1190/1.1988182

 Zhang Y, Xu S, Bleistein N, Zhang G. True-amplitude, angle-domain, common-image gathers from one-way waveequation migrations. *Geophysics*. 2007;72(1):S49-S58.

doi: 10.1190/1.2399371

9. Baysal E, Kosloff DD, Sherwood JW. Reverse time migration. *Geophysics*. 1983;48(11):1514-1524.

doi: 10.1190/1.1441434

 McMechan GA. Migration by extrapolation of timedependent boundary values. Geophys Prospect. 2008;31: 413-420.

doi: 10.1111/j.1365-2478.1983.tb01060.x

 Whitmore ND. Iterative depth migration by backward time propagation. In: SEG Technical Program Expanded Abstracts. Las Vegas, NV, USA: Society of Exploration Geophysicists; 1983. p. 382-385.

doi: 10.1190/1.1893867

12. Nguyen BD, McMechan GA. Five ways to avoid storing source wavefield snapshots in 2D elastic prestack reverse time migration. *Geophysics*. 2015;80(1):S1-S18.

doi: 10.1190/geo2014-0014.1

 Bo F, Huazhong W. Reverse time migration with source wavefield reconstruction strategy. *J Geophys Eng.* 2012;9(1):69-74.

doi: 10.1088/1742-2132/9/1/008

14. Liu S, Li X, Wang W, Zhu T. Source wavefield reconstruction using a linear combination of the boundary wavefield in reverse time migration. *Geophysics*. 2015;80(6):S203-S212.

doi: 10.1190/geo2015-0109.1

 Nguyen BD, McMechan GA. Excitation amplitude imaging condition for prestack reverse-time migration. *Geophysics*. 2013;78(1):S37-S46.

doi: 10.1190/geo2012-0079.1

 Zhang M, Zhou H, Chen H, Jiang S, Jiang C. Reverse-time migration using local Nyquist cross-correlation imaging condition. *IEEE Trans Geosci Remote Sens*. 2022;60:1-14.

doi: 10.1109/TGRS.2022.3168582

 Wang J, Li Q, Qiao B, Qi J. Reverse time migration using excitation amplitude imaging condition based on accurate first-arrival traveltimes calculation. *IEEE Trans Geosci Remote Sens*. 2025;63:1-11

doi: 10.1109/TGRS.2025.3527144

 Wang W, McMechan GA. Vector-based elastic reverse time migration. Geophysics. 2015;80(6):S245-S258.

doi: 10.1190/geo2014-0620.1

19. Zhou J, Wang D. Vector-based excitation amplitude imaging condition for elastic RTM. *J Appl Geophys*. 2017;147:1-9.

doi: 10.1016/j.jappgeo.2017.10.003

 Kalita M, Alkhalifah T. Efficient full waveform inversion using the excitation representation of the source wavefield. *Geophys J Int.* 2017;210(3):1581-1594.

doi: 10.1093/gji/ggx214

 Oh JW, Kalita M, Alkhalifah T. 3D elastic fullwaveform inversion using P-wave excitation amplitude: Application to ocean bottom cable field data. Geophysics. 2018;83(2):R129-R140.

doi: 10.1190/geo2017-0236.1

- 22. Lee D, Kang SG, Kim S, Kim YS, Chung W. Efficient direct envelope inversion with excitation amplitude for strong velocity contrast model. *IEEE Trans Geosci Remote Sens*. 2024;62:1-12.
 - doi: 10.1109/TGRS.2024.3422978
- 23. Kim S, Kim YS, Chung W. Least-squares reverse time migration using the most energetic source wavefields based on excitation amplitude imaging condition. *Geophys Prospect*. 2023;71(8):1438-1454.

doi: 10.1111/1365-2478.13387

- 24. Kim S, Kang SG, Choi Y, Chung W. Efficient extended least-squares reverse time migration based on an excitation amplitude imaging condition. *Geophysics*. 2024;89(1): S31-S45.
 - doi: 10.1190/geo2023-0216.1
- 25. Komatitsch D, Martin R. An unsplit convolutional perfectly matched layer improved at grazing incidence for the seismic wave equation. *Geophysics*. 2007;72(5):SM155-SM167.
 - doi: 10.1190/1.2757586
- 26. Yoon K, Suh S, Cai J, Wang B. Improvements in Time Domain FWI and Its Applications. In: *SEG International Exposition and Annual Meeting*. 2012. p. 1-5.

doi: 10.1190/segam2012-1535.1

Appendix

(A) Derivation of Equation XV

Using the properties of the dot product, **Equation XIV** can be written as follows:

$$I_{e}(\mathbf{x}) = \mathbf{u}_{e}, \mathbf{W}^{T} \mathbf{R} \mathbf{V}_{e} \mathbf{R} \mathbf{d}. \#$$
 (A.I)

Operator W^TR in the right operand in the dot product (**Equation A. I**) acts as a cross-correlation of the source wavelet with flipped input signal. It is also same as the flipped result of convolution between flipped source wavelet and input signal, which can be expressed as RW. Thus, **Equation A. I** can be rewritten as follows:

$$W^{T} RV^{\delta} Rd = RWV^{\delta} Rd.#$$
(A.II)

In above equation, since W and V^{δ} are causal convolution operators, order of operator WV^{δ} can be exchanged as V^{δ} W. Furthermore, based on the same manner as operator $W^{T}R$, the right hand side of **Equation A. II** can be modified as follows:

$$RWV^{\delta} Rd$$

$$=RV^{\delta} WRd$$

$$=V_{.}^{T}RWRd$$

$$=V_{.}^{T}RRW^{T}d$$

$$=V_{.}^{T}W^{T}d.#$$
(A.III)

Since time-reverse operator R is involutory matrix, which has its own inverse, RR becomes identity matrix I. Finally, **Equation XV** is obtained.

(B) Algorithm

Algorithm 1. Wave equation-based migration approach using interpolated excitation information

```
Migration velocity model c, recorded seismogram d, source wavelet f(t), source and receiver position x_a and x_b, arbitrary source position x^a
Output: Migration image I (x)
           for x_a \in x_a do
2:
           Forward wavefield simulation at x
           While t < T do
3:
4:
           if |S(t, x; x_a)| \ge |A(x; x_a)| then
5:
6:
7:
                          A(\mathbf{x}; \mathbf{x}_a) = S(t_{ex}, \mathbf{x}; \mathbf{x}_a)
           End if
8:
           End while
9:
10:
           End for
11:
           Interpolate excitation information
12:
           For x_i \in x_i do
           Construct causal convolution matrix W using f(t)
13:
           For x_r \in x_r do
14:
                      \hat{\mathbf{d}} = \mathbf{W}^T \mathbf{d}
15:
           Calculate migration image I_e(\mathbf{x}; \mathbf{x}_s) by Equation (XVI)
16:
                      I_e(\mathbf{x}) = I_e(\mathbf{x}) + I_e(\mathbf{x}; \mathbf{x}_s)
17:
           End for
18:
19:
           End for
```